

# Detecting Casimir torque with an optically levitated nanorod

Zhujiang Xu<sup>1</sup> and Tongcang Li<sup>1,2,3,4,\*</sup>

<sup>1</sup>*Department of Physics and Astronomy, Purdue University, West Lafayette, Indiana 47907, USA*

<sup>2</sup>*School of Electrical and Computer Engineering,*

*Purdue University, West Lafayette, Indiana 47907, USA*

<sup>3</sup>*Purdue Quantum Center, Purdue University, West Lafayette, Indiana 47907, USA*

<sup>4</sup>*Birck Nanotechnology Center, Purdue University, West Lafayette, Indiana 47907, USA*

(Dated: July 3, 2022)

The linear momentum and angular momentum of virtual photons of quantum vacuum fluctuations can induce the Casimir force and the Casimir torque, respectively. While the Casimir force has been measured extensively, the Casimir torque has not been observed experimentally though it was predicted over forty years ago. Here we propose to detect the Casimir torque with an optically levitated nanorod near a birefringent plate in vacuum. The axis of the nanorod tends to align with the polarization direction of the linearly polarized optical tweezer. When its axis is not parallel or perpendicular to the optical axis of the birefringent crystal, it will experience a Casimir torque that shifts its orientation slightly. We calculate the Casimir torque and Casimir force acting on a levitated nanorod near a birefringent crystal. We also investigate the effects of thermal noise and photon recoils on the torque and force detection. We prove that a levitated nanorod in vacuum will be capable of detecting the Casimir torque under realistic conditions.

## I. INTRODUCTION

A remarkable prediction of quantum electrodynamics (QED) is that there are an infinite number of virtual photons in vacuum due to the zero-point energy that never vanishes, even in the absence of electromagnetic sources and at a temperature of absolute zero. In 1948, Casimir predicted an attractive force between two ideal metal plates due to the linear momentum of virtual photons [1]. The number of electromagnetic modes between two metal plates is less than the number of modes outside the plates, thus the plates experience an attractive force, which is Casimir force. Casimir force has already been measured many times throughout the years [2–10]. Besides the linear momentum, the angular momentum carried by photons can generate the Casimir torque (or van der Waals torque) for anisotropic materials[11–13]. Despite significant interests about the Casimir torque [14–21], the torque has not been measured experimentally though it was predicted over 40 years ago, mainly due to the lack of a suitable tool [7–10].

Here we propose a method to measure the Casimir torque with a nanorod levitated by a linearly polarized optical tweezer in vacuum near a birefringent plate. The relative orientation between the nanorod and the birefringent crystal could be manipulated by the polarization of the trapping laser beam. When the long axis of the nanorod is not aligned with a principle axis of the birefringent plate, there will be a Casimir torque acting on the nanorod, which tries to minimize the energy, as shown in FIG. 1. Here  $d$  is the separation between the nanorod and the plate, and  $\theta$  is the angle between the long axis of the nanorod and the optical axis of the birefringent plate. Casimir torque is related to separation

$d$  and relative orientation  $\theta$ , which will be shown in the next section.

An optically levitated nanoparticle in vacuum can have an ultrahigh mechanical quality factor ( $Q > 10^9$ ) as it is well-isolated from the thermal environment, which is excellent for precision measurements [22–34]. Optical levitation of a silica ( $\text{SiO}_2$ ) nanosphere in vacuum at  $10^{-8}$  torr [34], and force sensing at  $10^{-21}$  N level with a levitated nanosphere [33] have been demonstrated in two separate experiments. The libration of an optically levitated nonspherical nanoparticle in vacuum has also been observed [25, 32], which provides a solid foundation for this proposal. Here we show that a silica nanorod with a length of 200 nm and a diameter of 40 nm levitated in vacuum at  $10^{-7}$  torr will have torque detection sensi-

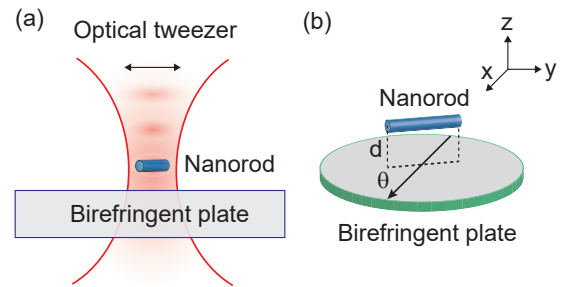


FIG. 1. (a) A nanorod levitated by a linearly polarized optical tweezer in vacuum near a birefringent plate. Its axis tends to align with the polarization direction of the optical tweezer. (b) There will be a Casimir torque on the nanorod when its axis is not aligned with a principle axis (the black arrow) of the birefringent plate. The trapping laser beam can also be used as the detecting beam to measure the torsional motion of the nanorod. Here  $d$  is the separation between the nanorod and the plate, and  $\theta$  is the angle between the long axis of the nanorod and the optical axis of the birefringent plate.

\* Corresponding author: tcli@purdue.edu

tivity about  $10^{-28}$  Nm/ $\sqrt{\text{Hz}}$  at room temperature. The Casimir torque between a nanorod with the same size and a birefringent plate separated by 266 nm is calculated to be on the order of  $10^{-25}$  Nm. The Casimir torque is 3 orders of magnitude larger than the minimum torque we can detect in 1 second, and thus will be detectable with our system. A levitated nanorod in vacuum will be several orders more sensitive than the state-of-the-art torque sensor. The best reported torque sensitivity is  $2.9 \times 10^{-24}$  Nm/ $\sqrt{\text{Hz}}$ , which was achieved by cooling a cavity-optomechanical torque sensor to 25mK in a dilution refrigerator [35]. The force detection sensitivity will be limited by the thermal noise when the pressure is above  $10^{-7}$  torr. When the pressure is below  $10^{-7}$  torr, the force sensitivity is mainly limited by photon recoil, which is about  $10^{-21}$  N/ $\sqrt{\text{Hz}}$ . Our calculated turning point of the force sensitivity around  $10^{-7}$  torr is consistent with the experimental observation of photon recoils around  $10^{-7}$  torr [34]. The exact turning point depends on the size and shape of the nanoparticle, as well as the intensity of the trapping laser.

Compared to the recent proposal of detecting the effects of Casimir torque with a liquid crystal [20], our method with a levitated nanorod in vacuum will be able to measure the Casimir torque at a much larger separation ( $d > 200$  nm), where retardation is significant. We will also be able to investigate the Casimir torque as a function of relative orientation in detail.

## II. TRAPPING POTENTIAL

We consider a silica nanorod with a length of  $l = 200$  nm in the long axis and a diameter of  $2a = 40$  nm trapped with a linearly polarized Gaussian beam in vacuum. The electric field of the beam can be described under the paraxial approximation as

$$E_x(x, y, z) = E_0 \frac{\omega_0}{\omega(z)} \exp\left\{\frac{-(x^2 + y^2)}{[\omega(z)]^2}\right\} \times \exp(ikz + ik\frac{x^2 + y^2}{2R(z)} - i\zeta(z)), \quad (1)$$

$$E_y(x, y, z) = E_z(x, y, z) = 0, \quad (2)$$

where  $E_0$  is the electric field amplitude at the origin,  $\omega(z)$  is the radius at which the field amplitudes fall to  $1/e$  of their axial values at the plane  $z$  along the beam,  $R(z)$  is the radius of curvature of the beam's wavefronts at  $z$  and  $\zeta(z)$  is the Gouy phase at  $z$ .

In the case of rods with a large aspect ratio, the components of the polarizability tensor [31] parallel and perpendicular to the symmetry axis are  $\alpha_{\parallel} = V\epsilon_0(\epsilon_r - 1)$  and  $\alpha_{\perp} = 2V\epsilon_0(\epsilon_r - 1)/(\epsilon_r + 1)$ . Here  $V$  is the volume of the object and  $\epsilon_r$  is the relative permittivity of the object. The absorption of electromagnetic field of the silica is negligible, so we assume  $\epsilon_r$  is real. When the size of the nanorod is much smaller than the wavelength of the laser (here we choose wavelength as 1064 nm), we can apply

the Rayleigh approximation. The induced dipole will be  $\mathbf{p} = \alpha_x E_x \hat{\mathbf{x}}_N + \alpha_y E_y \hat{\mathbf{y}}_N + \alpha_z E_z \hat{\mathbf{z}}_N$ , where the instantaneous electric field of the laser beam  $\mathbf{E}$  is decomposed into components along the principle axes of the nanorod. The long axis of the nanorod will tend to align with the polarization of the laser. When the vibration amplitude is small, the optical potential is harmonic around the laser focus and the vibrations of the trapped nanorod along different directions are uncoupled. Here we focus on its motion of the center of mass along  $z$  axis and its rotation around  $z$  axis. Thus the potential energy of the nanorod in the optical tweezer is

$$U(z, \phi) = -\frac{1}{2c\epsilon_0} [\alpha_{\parallel} - (\alpha_{\parallel} - \alpha_{\perp}) \sin^2 \phi] I_{laser}(z), \quad (3)$$

where  $c$  is the speed of light,  $\epsilon_0$  is the vacuum permittivity,  $\phi$  is the angle between the long axis of the nanorod and the polarization of the Gaussian beam, and  $I_{laser}(z)$  is the laser intensity at the location of the nanorod. In free space, the peak laser intensity at the focus is given

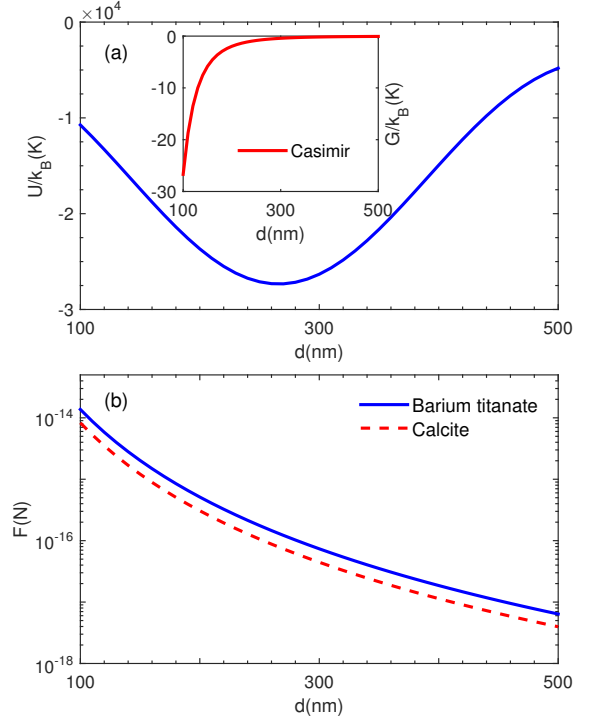


FIG. 2. (a) Calculated trapping potential for a silica nanorod with a length of 200 nm and a diameter of 40 nm as a function of separation  $d$ . Here we set the center of Gaussian beam at  $d = 266$  nm, laser power as 100 mW and laser waist radius as 400 nm. Inset: Calculated Casimir free energy in 300 K as a function of separation  $d$  at relative orientation  $\theta = \pi/4$ . Here we choose the substrate material to be barium titanate. (b) Calculated Casimir force at 300 K as a function of separation  $d$  between the silica nanorod and a birefringent crystal at relative orientation  $\theta = \pi/4$ . The blue solid line and red dashed line represent the Casimir force when the birefringent crystals are barium titanate and calcite, respectively.

by  $I_{laser} = Pk_0^2 NA^2 / (2\pi)$ , where  $P$  is the laser power,  $NA$  is the numerical aperture of the objective lens, and  $k_0$  is the magnitude of the wave vector of the laser beam. We assume  $NA = 0.85$  in this paper.

Here we also need to consider the reflection from the substrate, which will form a standing wave with the incident wave and strengthen the trapping potential at the  $1/4$  wavelength point (FIG. 1). We assume that the center of Gaussian beam is  $1/4$  wavelength away from the surface of the substrate. In our case, the wavelength is 1064 nm, so the center of the beam will be 266 nm from the substrate surface. The refractive index is  $n_0 = 1$  for vacuum and are  $n_o = 2.269$  and  $n_e = 2.305$  for ordinary and extraordinary axis of the birefringent crystal ( $BaTiO_3$ ) at 1064 nm[36], respectively. If the laser is perpendicular to the surface, the reflectance along ordinary and extraordinary axis are  $R_o = 0.16$  and  $R_e = 0.15$ . For a laser beam focused by a  $NA = 0.85$  objective lens, the angular aperture is  $58^\circ$ . The angle of incidence varies a lot at the surface of birefringent crystal and then the reflectance will become location and orientation dependent. However, only reflected wave from light with a small incident angle will interfere with the incident wave and contributes to the trapping potential near  $z$  axis, where the nanorod is trapped. Furthermore, when a linearly polarized laser beam is focused before hitting a surface, 50% of the laser will be parallel to the incident plane ( $p$ -polarized), while the other 50% of the laser will be perpendicular to the incident plane ( $s$ -polarized). The average reflectance of a 50%  $p$ -polarized and 50%  $s$ -polarized laser at the maximum incident angle  $58^\circ$  is 0.19, which is still close to  $R_o = 0.16$  and  $R_e = 0.15$ . Therefore, we use  $R_o$  and  $R_e$  in the calculation for simplicity.

We assume that the linearly polarized laser is polarized at  $\pi/4$  relative to both optical axes of the birefringent crystal, and the axis of the nanorod is aligned with the polarization of the Gaussian beam ( $\phi \approx 0$ ), then the potential near  $z = 0$  (or  $d = d_0$ ) is modified by

$$U(z) \approx -\frac{1}{4}\alpha_{\parallel} E_0^2 \left[ \frac{\omega_0^2}{[\omega(z)]^2} + \frac{R_o + R_e}{2} \frac{\omega_0^2}{[\omega(2d_0 - z)]^2} - (\sqrt{R_o} + \sqrt{R_e}) \times \cos(2kz) \frac{\omega_0^2}{\omega(z)\omega(2d_0 - z)} \right], \quad (4)$$

where  $d_0 = 266$  nm is the distance from the center of the Gaussian beam to the birefringent crystal. We use Eq. 4 to calculate the trapping potential and the result is shown in FIG. 2 (a). Here the laser power is 100 mW and the waist radius is approximately 400 nm. The potential energy at the center of the beam is around  $2.7 \times 10^4 K$ , which allow us to avoid losing the nanorod from thermal motion at room temperature.

### III. CASIMIR INTERACTION

Casimir forces and van der Waals forces have the same physical origin, as they both arise from quantum fluctuations. Casimir forces between macroscopic surfaces involve separations typically larger than 100 nm where retardation effect plays an important role, while van der Waals forces often refer to separations smaller than a few nm where retardation is negligible[7–10]. To calculate the Casimir interaction between a nanorod and a birefringent plate, we follow the method in Ref. [17, 37] by assuming that a half space is a dilute assembly of anisotropic cylinders. With that we could extract the interaction between a cylinder and one semi-infinite half space from the interaction free energy between two half spaces. We notice that Ref. [17] has two typos. In Eq. 5 about the function  $N$  in Ref. [17], the first term in the third line, should be  $\rho_3^2(\epsilon_3 - \epsilon_{1,\perp})(Q^2 + \rho_{1,\perp}\rho_3)$  instead of  $\rho_3^3(\epsilon_3 - \epsilon_{1,\perp})(Q^2 + \rho_{1,\perp}\rho_3)$ . In Eq. 7 for the function  $\tilde{f}(\phi)$  in Ref. [17], the term inside the square root should be  $Q^2((\epsilon_{1,\parallel}/\epsilon_{1,\perp}) - 1) \cos^2 \phi + \rho_{1,\perp}^2$  instead of  $Q^2((\epsilon_{1,\parallel}/\epsilon_{1,\perp}) - 1) \cos^2 \phi + \rho_{1,\parallel}^2$ . The corrected interaction free energy per unit length of the cylinder,  $g(d, \theta)$ , between a single cylinder and a half-space substrate is

$$g(d, \theta) = \frac{k_B T a^2}{4\pi} \sum_{n=0}^{\infty} \int_0^{\infty} Q dQ \int_0^{2\pi} d\phi \left[ e^{-2d\rho_3} \frac{N}{D} \right], \quad (5)$$

where

$$\begin{aligned} N = & \left( \frac{\Delta_{\parallel}}{2} - \Delta_{\perp} \right) \{ Q^2 \sin^2(\phi + \theta) \times [\tilde{f}(\phi)\epsilon_{1,\perp}(Q^2 \sin^2 \phi (\rho_{1,\perp} + \rho_3) + \rho_{1,\perp}\rho_3(\rho_3 - \rho_{1,\perp})) + (\epsilon_{1,\perp} - \epsilon_3)(\rho_3(\rho_{1,\perp} + 2\rho_3) \\ & - Q^2)] - 2\tilde{f}(\phi)\epsilon_{1,\perp}\rho_{1,\perp}\rho_3^2[2Q^2 \sin \phi \cos \theta \sin(\phi + \theta) + \rho_3^2 \sin^2 \theta] + \tilde{f}(\phi)\epsilon_{1,\perp}\rho_3^2[Q^2 \sin^2 \phi (\rho_{1,\perp} - \rho_3) + \rho_{1,\perp}\rho_3(\rho_{1,\perp} + \rho_3)] \\ & + \rho_3^2(\epsilon_3 - \epsilon_{1,\perp})(Q^2 + \rho_{1,\perp}\rho_3) \} + 2\tilde{f}(\phi)\Delta_{\perp}\epsilon_{1,\perp}[Q^2 \sin^2 \phi (Q^2 \rho_{1,\perp} - \rho_3^2) + \rho_{1,\perp}\rho_3^2(Q^2 \cos(2\phi) + \rho_{1,\perp}\rho_3)] \\ & - \Delta_{\perp}(\epsilon_{1,\perp} - \epsilon_3) \times [(Q^2 + \rho_3^2)(Q^2 + \rho_{1,\perp}\rho_3) + (Q^2 - \rho_3^2)(Q^2 - \rho_{1,\perp}\rho_3)] \end{aligned} \quad (6)$$

and

$$D = \rho_3(\rho_{1,\perp} + \rho_3) \{ \epsilon_{1,\perp} \tilde{f}(\phi) [Q^2 \sin^2 \phi - \rho_{1,\perp}\rho_3] + \epsilon_{1,\perp}\rho_3 + \epsilon_3\rho_{1,\perp} \}. \quad (7)$$

In the equations above,

$$\rho_{1,\perp} = \sqrt{Q^2 + \frac{\epsilon_{1,\perp}\omega_n^2}{c^2}}, \quad (8)$$

$$\rho_3 = \sqrt{Q^2 + \frac{\epsilon_3 \omega_n^2}{c^2}}, \quad (9)$$

$$\tilde{f}(\phi) = \frac{\sqrt{Q^2((\epsilon_{1,\parallel}/\epsilon_{1,\perp}) - 1) \cos^2 \phi + \rho_{1,\perp}^2 - \rho_{1,\perp}}}{Q^2 \sin^2 \phi - \rho_{1,\perp}^2}. \quad (10)$$

Here  $\Delta_{\perp} = (\epsilon_{2,\perp} - \epsilon_3)/(\epsilon_{2,\perp} + \epsilon_3)$ ,  $\Delta_{\parallel} = (\epsilon_{2,\parallel} - \epsilon_3)/\epsilon_3$  are the relative anisotropy measures of the cylinder,  $d$  is the separation between the cylinder and the half-space,  $a$  is the radius of the cylinder,  $k_B$  is Boltzmann constant,  $T$  is temperature,  $\epsilon_3$  is the dielectric response of the isotropic medium between the cylinder and the half space,  $\epsilon_{1,\perp}$  and  $\epsilon_{1,\parallel}$  are the dielectric responses of the birefringent material,  $\epsilon_{2,\perp}$  and  $\epsilon_{2,\parallel}$  are the dielectric responses of the cylinder material. Subscript  $n$  is the index for the Matsubara frequencies, which are  $\omega_n = 2n\pi k_B T/\hbar$ , and the prime on the summation in Eq. 5 means that the weight of the  $n = 0$  term is  $1/2$ . All the dielectric responses should be considered as functions of discrete imaginary Matsubara frequencies, i.e., as  $\epsilon_3 \equiv \epsilon_3^{(n)} = \epsilon_3(i\omega_n)$ ,  $\epsilon_{1,\perp}(i\omega_n)$ ,  $\epsilon_{1,\parallel}(i\omega_n)$ ,  $\epsilon_{2,\perp}(i\omega_n)$  and  $\epsilon_{2,\parallel}(i\omega_n)$ .

The dielectric properties of many materials are well described by a multiple oscillator model (the so-called Ninham-Parsegian representation)[38]. For most inorganic materials, only two undamped oscillators are commonly used to describe the dielectric function[39, 40],

$$\epsilon(i\xi) = 1 + \frac{C_{IR}}{1 + (\xi/\omega_{IR})^2} + \frac{C_{UV}}{1 + (\xi/\omega_{UV})^2}, \quad (11)$$

where  $\omega_{IR}$  and  $\omega_{UV}$  are the characteristic absorption angular frequencies in the infrared and ultraviolet range, respectively, and  $C_{IR}$  and  $C_{UV}$  are the corresponding absorption strengths. For the birefringent materials, there are separate functions describing dielectric functions for the ordinary and extraordinary axis. The model parameters used for our calculations are summarized in Table I.

We could use Eq. 5- 11 and parameter data in Table I to calculate the Casimir free energy  $G(d, \theta) = g(d, \theta) \times l$ , where  $l$  is the length of the cylinder [41]. FIG. 2.(a) inset shows that the Casimir free energy is very small for separation  $d > 100$  nm, compared to the optical trapping potential. So the nanorod will be trapped near the

center of the laser beam without being attracted to the substrate by the Casimir force. When  $d < 100$  nm the size of the nanorod is comparable to the separation between the nanorod and the birefringent crystal, thus the dilute cylinder approximation will fail. Therefore, we only consider the situation when  $d > 100$  nm.

Then the retarded Casimir (or Casimir-Lifshitz) force is given by

$$F = -\frac{\partial G(d, \theta)}{\partial d}, \quad (12)$$

and the torque induced by the birefringent plates is given by [12]

$$M = -\frac{\partial G(d, \theta)}{\partial \theta}. \quad (13)$$

Using Eq. 12, 13, we have calculated the Casimir force and torque expected for different separations at relative orientation  $\theta = \pi/4$ , both for the barium titanate and calcite as the birefringent crystal. The results obtained for  $T = 300$  K are reported in FIG. 2.(b) and FIG. 3.(a). The force and torque both decrease as the separation increases, the force follows the same power dependence of the separation for different birefringent materials. However, there is no single power law dependence that describes the torque at all separations regardless of the choice of materials. That is because the torque is directly determined by the dielectric response difference between ordinary and extraordinary axes, which is discrepant between barium titanate and calcite (in Table.1).

We have also calculated the Casimir torque at  $d = 266$  nm as a function of the relative orientation. From the results reported in FIG. 3.(b), one can clearly see that the torque oscillates sinusoidally with periodicity of

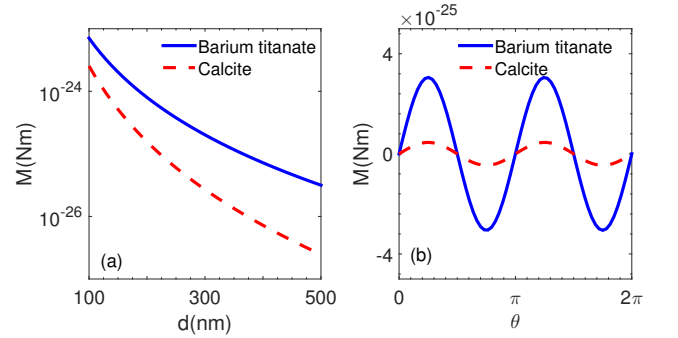


TABLE I. Model parameters used to determine the dielectric function of the materials[14, 39, 40].

	$C_{IR}$	$C_{UV}$	$\omega_{IR}(\text{rad/s})$	$\omega_{UV}(\text{rad/s})$
Calcite $_{\parallel}$	5.300	1.683	$2.691 \times 10^{14}$	$1.660 \times 10^{16}$
Calcite $_{\perp}$	6.300	1.182	$2.691 \times 10^{14}$	$2.134 \times 10^{16}$
Barium titanate $_{\parallel}$	3595	4.128	$0.850 \times 10^{14}$	$0.841 \times 10^{16}$
Barium titanate $_{\perp}$	145.0	4.064	$0.850 \times 10^{14}$	$0.896 \times 10^{16}$
Silica	0.829	1.098	$0.867 \times 10^{14}$	$2.034 \times 10^{16}$

FIG. 3. (a) Calculated Casimir torque in 300K as a function of separation  $d$  between the silica nanorod ( $l = 200$  nm,  $a = 20$  nm) and a birefringent crystal at relative orientation  $\theta = \pi/4$ . The blue solid line and red dashed line represent the torque when the birefringent crystals are barium titanate and calcite, respectively. (b) Calculated Casimir torque in 300K as a function of relative orientation  $\theta$  between the silica nanorod ( $l = 200$  nm,  $a = 20$  nm) and a birefringent crystal by a separation  $d = 266$  nm. The blue solid line and red dashed line represent the torque when the birefringent crystals are barium titanate and calcite, respectively.

$\pi$ :  $M = M_0 \sin(2\theta)$ . The maximum magnitude of the torque occurs at  $\theta = \pi/4$  and  $\theta = 3\pi/4$ . For different birefringent crystals, the maximum magnitudes of the torque are different, but have the same periodicity. As expected, materials with less birefringence give rise to a smaller torque. Thus Casimir torque between silica nanorod and calcite is smaller than that with barium titanate.

#### IV. EFFECTS OF THERMAL PHOTONS

Several papers have reported measurements of the thermal Casimir force [42, 43], which is due to thermal photons (blackbody radiation) at finite temperature rather than quantum vacuum fluctuations of the electromagnetic field. At room temperature, the thermal Casimir force is typically much smaller than the conventional Casimir force due to quantum vacuum fluctuations. The measurements of thermal Casimir force could test different models of materials. In fact, it is still under debate about how to calculate the thermal Casimir force between real materials [44]. It is thus interesting to see how thermal photons affect the Casimir torque and whether thermal Casimir torque will be detectable with our proposed method.

When the separation between the nanorod and the birefringent crystal is relatively small and the temperature is relatively low, the blackbody radiation could be neglected. But when the temperature and the separation increase, a small fraction of the torque will come from thermal photons. To single out the effects of thermal photons, we assume the dielectric functions of materials are independent of temperature. The effect of temperature is only included in the Bose-Einstein distribution of thermal photons. In other words, we let the explicit temperature  $T$  in Eq. 5 and the Matsubara frequencies  $\omega_n = 2n\pi k_B T / \hbar$  be a variable, while assuming all parameters listed in Table 1 to be constants. While this is a crude approximation, it can help us to understand the effects of thermal photons on the Casimir torque. In real experiments, the properties of materials will depend on temperature. So the situation will be more complex.

The calculated results of the Casimir force and torque as a function of temperature are shown in FIG. 4.(a)-(d). We can see that the thermal Casimir effect is very small (less than a few percent). So the measured torque will mainly come from quantum fluctuations. The purpose of this calculation is to estimate the magnitude of the effect of thermal photons. Since we did not consider the change of the dielectric constants of the real materials as a function of temperature, the temperature dependence of the experimental results is expected to be different from FIG. 4. To avoid complications, it will be better to do the experiment at a fixed temperature. Because the effect of thermal photons is very small, the measured temperature dependence of the Casimir torque will be most likely due to the temperature dependence of the

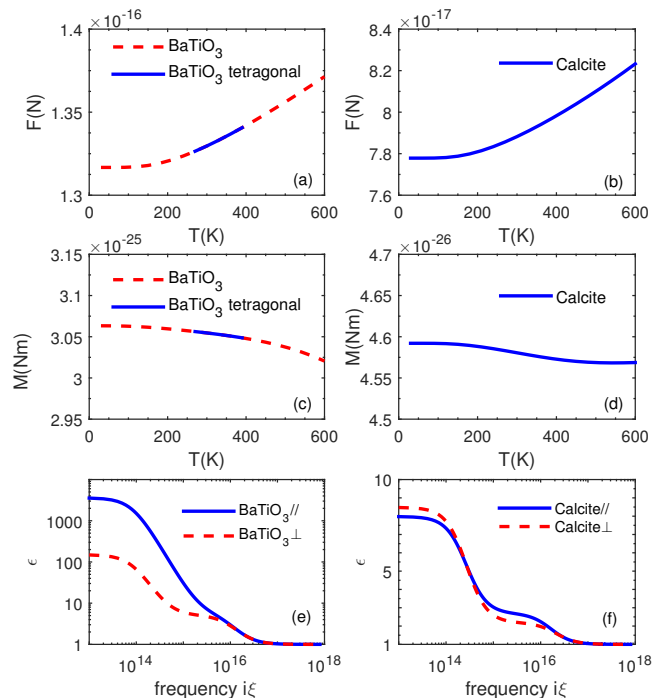


FIG. 4. (a),(b) Calculated temperature dependence of Casimir force between a silica nanorod and a birefringent crystal, separated with a distance of 266 nm and aligned with an angle of  $\pi/4$ . The materials of the birefringent crystals are barium titanate and calcite, respectively. To single out the effects of thermal photons, we did not consider the temperature dependence of dielectric parameters in the calculation. When the temperature is below 400K, the force is almost unchanged, with only 2 % difference. As the temperature increases, the casimir force increases and temperature dependence becomes more and more significant. For barium titanate, the temperature range for tetragonal structure is 278K-393K, the blue solid line represents this range. Calcite is a very stable birefringent crystal during the plotted temperature range. (c),(d) Calculated temperature dependence of Casimir torque. When the temperature is below 400K, the torque is almost unchanged. As the temperature increases, the casimir torque decreases and temperature dependence becomes more and more significant. (e),(f) Dielectric functions as a function of imaginary angular frequency for barium titanate and calcite. Blue solid lines and red dashed lines represent,  $\epsilon_{||}$  and  $\epsilon_{\perp}$ , respectively.

dielectric functions, instead of thermal photons.

#### V. TORQUE MEASUREMENT METHOD

To measure the Casimir torque, we will need to cancel out other torques on the nanorod. Since the reflectances along the ordinary and extraordinary axis are different, the reflected light will not have the same polarization as the incident light. Thus there will be an optical torque



from the laser reflected by the birefringent plate. To eliminate this effect, we will switch the optical tweezer on and off repeatedly to detect the Casimir torque by observing the rotation of the nanorod. We could extract the contribution to the rotation which solely comes from the Casimir effect during the period when the laser is off. If the nanorod has a permanent electric or magnetic dipole, there may also be a torque on the nanorod due to stray electric or magnetic fields. Different from Casimir torque, such torque due to a permanent dipole has a period of  $2\pi$ . So if we rotate the nanorod by  $180^\circ$ , the permanent torque will change its sign, while the Casimir torque will be the same (FIG. 3.(b)). Thus we can cancel out other torques on the nanorod by a careful design.

For  $d = 266$  nm, the maximum magnitude of the torque is around  $3.2 \times 10^{-25}$  Nm for barium titanate and around  $6 \times 10^{-26}$  Nm for calcite. In order to prove that our optically levitated nanorod system is able to detect the Casimir force and torque, we also calculated the sensitivity of the force and the torque.

### A. Torque sensitivity

To understand the limit of torque sensitivity in the quantum regime, one must consider the noise limit which comes from thermal fluctuations, as well as from photon recoil. In air, the interaction between the nanorod and the thermal environment dominates the noise, thus the photon recoil from the laser can be neglected. However, in high vacuum, the dominant source of noise can come from the unavoidable photon recoil in the optical trap and sets an ultimate bound for the sensitivity.

For small oscillation amplitudes, the equation of motion of a harmonic torsional oscillator is

$$\ddot{\theta} + \gamma\dot{\theta} + \Omega_r^2\theta = M(t)/I, \quad (14)$$

where  $\theta$  is the angular deflection of the oscillator,  $\Omega_r$  is the frequency of rotational motion,  $M$  is a fluctuating torque,  $I$  is the moment of inertia around the torsion axis, and  $\gamma$  is the damping rate of the torsional motion which can be written as  $\gamma = \gamma_{th} + \gamma_{rad}$ . Here  $\gamma_{th}$  accounts for the interaction with the background gas,  $\gamma_{rad}$  refers to the interaction with the radiation field.

When the torque fluctuation is from Brownian noise, the angular fluctuations of an oscillator excited by such a stochastic torque could be calculated. The thermal noise limited minimum torque that can be measured with a torsion balance is [45]

$$M_{th} = \sqrt{\frac{4k_B T I \gamma_{th}}{\Delta t}}, \quad (15)$$

where  $k_B$  is the Boltzmann constant,  $T$  is the environment temperature, and  $\Delta t$  is the measurement time. The damping coefficient from thermal noise is  $\gamma_{th} = f_r/I$ .  $I = \frac{\rho\pi a^2 l^3}{12}$  is the moment of inertia of the nanorod around its center and perpendicular to its axis,  $\rho$  is the density of

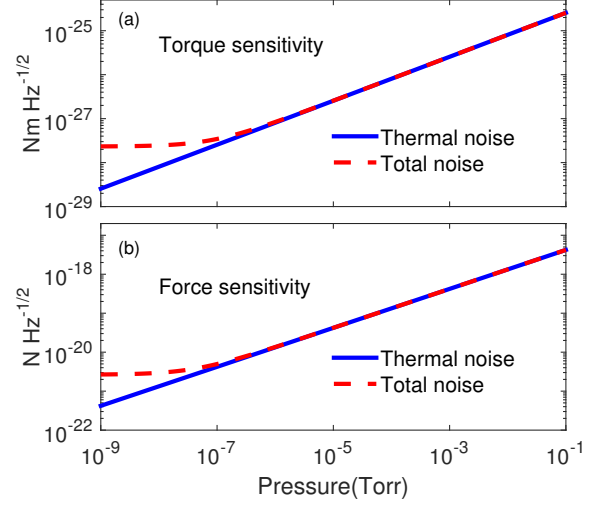


FIG. 5. (a) Calculated torque sensitivity limit of the rotational motion of a levitated silica nanorod ( $l = 200$  nm,  $a = 20$  nm) as a function of gas pressure. The blue solid line and the red dashed line represent the torque sensitivity limit due to only the thermal noise and due to both photon recoil and thermal noise. The laser power is 100 mW and the laser waist radius is 400 nm. (b) Calculated force sensitivity limit of the translational motion of a levitated Silica nanorod as a function of gas pressure. The blue solid line and the red dashed line represent the force sensitivity limit due to only the thermal noise and due to both photon recoil and thermal noise.

the nanorod,  $a$  is the nanorod radius and  $l$  is the nanorod length.  $f_r = k_B T / D_r$  is the rotational friction drag coefficient.  $D_r$  is the rotational diffusion coefficient for a rod in the free molecular regime and can be represented as [46]

$$D_r = k_B T K_n / \left\{ \pi \mu l^3 \left[ \left( \frac{1}{6} + \frac{1}{8\beta^3} \right) + f \left( \frac{\pi - 2}{48} + \frac{1}{8\beta} + \frac{1}{8\beta^2} + \frac{\pi - 4}{8} \frac{1}{8\beta^3} \right) \right] \right\}, \quad (16)$$

where  $\beta = l/a$  is the rod aspect ratio,  $K_n = \lambda/a$  is the Knudsen number,  $\lambda = \frac{\mu}{p} \sqrt{\frac{\pi k_B T}{2m_{gas}}}$  is the mean free path,  $m_{gas}$  is the molecular mass,  $\mu$  is the gas viscosity and  $f$  is the momentum accommodation, where we choose  $f = 0.9$ . Thus the minimum detectable torque due to thermal fluctuations  $M_{th}$  decreases with the square root of the measurement duration  $\Delta t$ , while increases with the square root of the pressure  $p$ .

Apart from fluctuations due to contact with the background gas, the unavoidable photon recoil from the optical trap also contributes to the noise limit. The shot noise due to photon recoil can be understood as momentum or angular momentum kicks from the scattered photons. The photon recoil limited minimum torque is

$$M_{rad} = \sqrt{\frac{4I}{\Delta t} \frac{d}{dt} K_R}, \quad (17)$$

where rotational shot noise heating rate of a nanorod from a linearly polarized trapping beam is [47–49]

$$\frac{d}{dt}\overline{K_R} = \frac{8\pi J_p}{3} \left( \frac{k_0^2}{4\pi\epsilon_0} \right)^2 (\alpha_\perp - \alpha_\parallel)^2 \frac{\hbar^2}{2I}. \quad (18)$$

Here the photon flux  $J_p$  is equal to the laser intensity over the energy of a photon, which means  $J_p = I_{laser}/\hbar\omega_0$ .  $\omega_0$  is the frequency of incident beam,  $k_0$  is the incoming wave vector. Therefore, the total torque limit is given by

$$M_{min} = \sqrt{M_{th}^2 + M_{rad}^2}, \quad (19)$$

We calculate the torque limit by using Eq. 15 - 19 and the result of the calculation is shown in FIG. 5.(a). The torque detection sensitivity of a levitated nanorod will be limited by the thermal noise when the pressure is above  $10^{-7}$  torr. When the pressure is below  $10^{-7}$  torr, the torque sensitivity is mainly limited by photon recoil. And when the pressure reaches  $10^{-8}$  torr, the torque sensitivity approaches the standard quantum limit, which is around  $10^{-28}$  Nm/ $\sqrt{\text{Hz}}$ . Thus the Casimir torque will be 3 orders larger than the minimum torque our system can detect in 1 second, and is expected to be measurable.

### B. Force sensitivity

Similar to the torque sensitivity, both thermal noise and photon recoil needs to be considered to determine force sensitivity. For small oscillation amplitudes, the nanorod's motion is described by three independent harmonic oscillators (for three directions), each with its own oscillation frequency  $\Omega_{0i}$  and damping rate  $\gamma_i$ , which is a result of the asymmetric shape of the optical potential. For example, the motion along y is described by,

$$\ddot{y} + \gamma_y \dot{y} + \Omega_{0y}^2 y = \frac{1}{m} F_y(t), \quad (20)$$

where  $y$  is the motion of the center of mass,  $m$  is the nanorod mass,  $F_y$  is a fluctuating force along y axis acting on the nanorod. The thermal noise limited minimum force in one direction  $i$  that can be measured with a force balance is

$$F_{th(i)} = \sqrt{\frac{4k_B T m \gamma_i}{\Delta t}}, \quad (21)$$

Here  $m$  is the mass,  $\gamma_i$  is the damping coefficient of the translational motion and depends on the velocity relative to the background gas. For anisotropic material, damping coefficients are directly related to the drag coefficients at each directions, which means that  $\gamma_\perp = K_\perp/m$  (component perpendicular to the axial direction) and  $\gamma_\parallel = K_\parallel/m$  (component parallel to the axial direction). In the free molecular regime, the drag force along different directions for a cylindrical particle are expressed by  $F_\perp = K_\perp V_\perp$  and  $F_\parallel = K_\parallel V_\parallel$  and drag coefficients are [50]

$$K_\perp = \frac{2\pi\mu a^2}{\lambda} \left[ \left( \frac{\pi-2}{4}\beta + \frac{1}{2} \right) f + 2\beta \right], \quad (22)$$

$$K_\parallel = \frac{2\pi\mu a^2}{\lambda} \left[ \left( \beta + \frac{\pi}{4} - 1 \right) f + 2 \right], \quad (23)$$

In our system, we only consider the motion perpendicular to the axis, which will affect the measurement of Casimir force. The force induced by thermal fluctuations is

$$F_{th} = \sqrt{\frac{4k_B T}{\Delta t}} K_\perp, \quad (24)$$

while the photon recoil limited minimum force is

$$F_{rad} = \sqrt{\frac{4m}{\Delta t}} \frac{d}{dt} \overline{K_T}. \quad (25)$$

Here the translational shot noise heating rate of a nanorod from a linearly polarized trapping beam is [47]

$$\frac{d\overline{K_T}}{dt} = \frac{8\pi J_p}{3} \left( \frac{k_0^2}{4\pi\epsilon_0} \right)^2 \alpha_\perp^2 \frac{\hbar^2 k_0^2}{2m}, \quad (26)$$

Therefore, the total force limit will be

$$F_{min} = \sqrt{F_{th}^2 + F_{rad}^2}, \quad (27)$$

Then we use Eq. 23- 27 to calculate the force sensitivity limit and the result is shown in FIG. 5.(b). The force detection sensitivity will be limited by the thermal noise when the pressure is above  $10^{-7}$  torr. When the pressure is below  $10^{-7}$  torr, the force sensitivity is mainly limited by photon recoil, which is about  $10^{-21}$  N/ $\sqrt{\text{Hz}}$ . The Casimir force is approximately  $10^{-16}$  N at  $d = 266$  nm, therefore, it is expected to be measurable.

## VI. CONCLUSION

In this paper, we show that the calculated Casimir force is on the order of  $10^{-16}$  N and the torque is on the order of  $10^{-25}$  Nm between an optically levitated silica nanorod ( $l = 200\text{nm}$ ,  $a = 20\text{nm}$ ) and a birefringent crystal separated by 266 nm. Considering noise from thermal interaction and photon recoil, we get the sensitivity of our system, which is on the order of  $10^{-28}$  Nm/ $\sqrt{\text{Hz}}$  at  $10^{-7}$  torr. Therefore, the system will allow us to measure the Casimir torque and test the fundamental prediction of quantum electrodynamics [2–13]. Besides its fascinating origin, the QED torque between anisotropic surfaces is expected to be important for the anisotropic growth of some crystals [21] and biological membranes. Our system will enable many other precision measurements, such as a measurement of the torque on a single nuclear spin [25].

## ACKNOWLEDGMENTS

We thank C. Zhong, F. Robicheaux, E. Fischbach, Z.-Q. Yin, J. Ahn, and J. Bang for helpful discussions. This work is partly supported by the National Science Foundation under grant No. PHY-1555035.

- 
- [1] H. B. G. Casimir, "On the attraction between two perfectly conducting plates", *Proc. K. Ned. Akad. Wet.* **51**, 793 (1948).
- [2] M. J. Sparnaay, "Measurements of attractive forces between flat plates", *Physica*, **24**, 751, (1958).
- [3] U. Mohideen and A. Roy. "Precision measurement of the Casimir force from 0.1 to 0.9  $\mu\text{m}$ ", *Phys. Rev. Lett.* **81**, 4549 (1998).
- [4] R. S. Decca, D. Lpez, E. Fischbach, D. E. Krause, "Measurement of the Casimir force between dissimilar metals", *Phys. Rev. Lett.* **91**, 050402, (2003)
- [5] J. N. Munday, F. Capasso, V. A. Parsegian, "Measured long-range repulsive Casimir-Lifshitz forces", *Nature* **457**, 170, (2009)
- [6] Y.-J. Chen, W. K. Tham, D. E. Krause, D. Lpez, E. Fischbach, R. S. Decca. "Stronger limits on hypothetical Yukawa interactions in the 30-8000 nm range", *Phys. Rev. Lett.* **116**, 221102, (2016)
- [7] J. N. Israelachvili, *Intermolecular and Surface Forces*. 3rd edition. (Elsevier, 2011) Chap. 13.
- [8] L. M. Woods, D. A. R. Dalvit, A. Tkatchenko, P. Rodriguez-Lopez, A. W. Rodriguez, and R. Podgornik, "Materials perspective on Casimir and van der Waals interactions", *Rev. Mod. Phys.* **88**, 045003 (2016).
- [9] F. Capassom J. N. Munday, D. Iannuzzi and H. B. Chan, "Casimir forces and quantum electrodynamical torques: physics and nanomechanics", *IEEE J. Sel. Top. Quant.* **13**, 400 (2007).
- [10] V. Mostepanenko, N. N. Trunov. "The Casimir effect and its applications" (Oxford University Press, New York, 1997).
- [11] V. A. Parsegian and G. H. Weiss, "Dielectric anisotropy and the van der Waals interaction between bulk media", *J. Adhes.* **3**, 259 (1972).
- [12] Y. S. Barash, "Moment of van der Waals forces between anisotropic bodies", *Radiophys. Quantum Electron.* **21**, 1138 (1978).
- [13] S. J. van Enk, "Casimir torque between dielectrics", *Phys. Rev. A* **52**, 2569 (1995).
- [14] J. N. Munday, D. Iannuzzi, Y. Barash, and F. Capasso, "Torque on birefringent plates induced by quantum fluctuations", *Phys. Rev. A* **71**, 042102 (2005).
- [15] J. N. Munday, D. Iannuzzi, and F. Capasso. "Quantum electrodynamical torques in the presence of Brownian motion", *New J. Phys.* **8**, 244 (2006).
- [16] X. Chen, J. C. H. Spence. "On the measurement of the Casimir torque", *Phys. Status Solidi B* **248**, 2064 (2011).
- [17] A. Šiber, R. F. Rajter, R. H. French, W. Y. Ching, V. A. Parsegian and R. Podgornik. "Optically anisotropic infinite cylinder above an optically anisotropic half space: Dispersion interaction of a single-walled carbon nanotube with a substrate", *J. Vac. Sci. Technol. B* **28**, C4A17 (2010).
- [18] A. Šiber, R. F. Rajter, R. H. French, W. Y. Ching, V. A. Parsegian, and R. Podgornik, "Dispersion interactions between optically anisotropic cylinders at all separations: Retardation effects for insulating and semiconducting single-wall carbon nanotubes", *Phys. Rev. B* **80**, 165414 (2009).
- [19] R. F. Rajter, R. Podgornik, V. A. Parsegian, R. H. French, and W. Y. Ching. "van der Waals - London dispersion interactions for optically anisotropic cylinders: Metallic and semiconducting single-wall carbon nanotubes", *Phys. Rev. B* **76**, 045417 (2007).
- [20] D. A. T. Somers, J. N. Munday, "Rotation of a liquid crystal by the Casimir torque", *Phys. Rev. A* **91**, 032520 (2015).
- [21] K. Yasui, K. Kato. "Oriented Attachment of Cubic or Spherical BaTiO<sub>3</sub> Nanocrystals by van der Waals Torque", *J. Phys. Chem. C* **119**, 24597 (2015).
- [22] Z.-Q. Yin, A. A. Geraci, T. Li. "Optomechanics of levitated dielectric particles". *Int. J. Mod. Phys. B* **27**, 1330018 (2013).
- [23] A. A. Geraci, S. B. Papp, J. Kitching. "Short-range force detection using optically cooled levitated microspheres", *Phys. Rev. Lett.* **105**, 101101 (2010).
- [24] T. Li, S. Kheifets, D. Medellin, M. G. Raizen. "Measurement of the instantaneous velocity of a Brownian particle", *Science*, **328**, 1673 (2010)
- [25] T. M. Hoang, Y. Ma, J. Ahn, J. Bang, F. Robicheaux, Z.-Q. Yin, T. Li. "Torsional optomechanics of a levitated nonspherical nanoparticle", *Phys. Rev. Lett.* **117**, 123604 (2016).
- [26] O. Romero-Isart, M. L. Juan, R. Quidant and J. Ignacio Cirac, "Toward quantum superposition of living organisms", *New J. Phys.* **12**, 033015 (2010).
- [27] D. E. Chang, C. A. Regal, S. B. Papp, D. J. Wilson, J. Ye, O. Painter, H. J. Kimble and P. Zoller, "Cavity opto-mechanics using an optically levitated nanosphere", *Proc. Natl. Acad. Sci. U.S.A.* **107**, 1005 (2010)
- [28] H. Shi and M. Bhattacharya, "Optomechanics based on angular momentum exchange between light and matter", *J. Phys. B: At. Mol. Opt. Phys.* **49** 153001 (2016).
- [29] H. Shi and M. Bhattacharya, "Coupling a small torsional oscillator to large optical angular momentum", *J. Mod. Opt.* **60**, 382 (2013).
- [30] T. Li, S. Kheifets and M. G. Raizen, "Millikelvin cooling of an optically trapped microsphere in vacuum", *Nat Phys.* **7**, 527 (2011).
- [31] B. A. Stickler, S. Nimmrichter, L. Martinetz, S. Kuhn, M. Arndt, and K. Hornberger, "Ro-translational cavity cooling of dielectric rods and disks", *Phys. Rev. A* **94**, 033818 (2016).
- [32] S. Kuhn, A. Kosloff, B. A. Stickler, F. Patolsky, K. Hornberger, M. Arndt, and J. Millen, "Full rotational control of levitated silicon nanorods", *Optica* **4**, **356** (2017)
- [33] G. Ranjit, M. Cunningham, K. Casey, A. A. Geraci, "Zeptonewton force sensing with nanospheres in an optical lattice", *Phys. Rev. A* **93**, 053801 (2016).
- [34] Vijay Jain, Jan Gieseler, Clemens Moritz, Christoph Delgado, Romain Quidant, and Lukas Novotny, "Direct measurement of photon recoil from a levitated nanoparticle", *Phys. Rev. Lett.* **116**, 243601 (2016).
- [35] P. H. Kim, B. D. Hauer, C. Doolin, F. Souris1 and J.P. Davis, "Approaching the standard quantum limit of mechanical torque sensing", *Nat. Commun.* **7**, 13165 (2016).
- [36] D. E. Zelmon, D. L. Small and P. Schunemann, "Refractive index measurements of barium titanate from .4 to 5.0 microns and implications for periodically poled frequency conversion devices", *Mat. Res. Soc. Symp. Proc.* **484**, 537 (1997)



- [37] V. A. Parsegian, “Van der Waals forces” (Cambridge University Press, Cambridge, 2005).
- [38] J. Mahanty and B. W. Ninham, “Dispersion forces” (Academic, London, 1976).
- [39] L. Bergstrom, “Hamaker constants of inorganic materials”, *Adv. Colloid Interface Sci.* **70**, 125 (1997).
- [40] D. B. Hough and L. R. White, “The calculation of Hamaker constants from Lifshitz theory with applications to wetting phenomena”, *Adv. Colloid Interface Sci.* **14**, 3 (1980).
- [41] V. M. Mostepanenko, N. N. Trunov. The Casimir effect and its applications. Pages 83-87 (Oxford University Press, New York, 1997).
- [42] A. O. Sushkov, W. J. Kim, D. A. R. Dalvit and S. K. Lamoreaux, “Observation of the thermal Casimir force”, *Nat. Phys.* **7**, 230 (2011) .
- [43] M. Bostrom and Bo E. Sernelius, “Thermal effects on the Casimir force in the  $0.1 - 5\mu\text{m}$  range”, *Phys. Rev. Lett.* **84**, 4757 (2000).
- [44] G. L. Klimchitskaya, M. Bordag, E. Fischbach, D. Krause, V. M. Mostepanenko, “Observation of the thermal Casimir force is open to question”, *Int. J. Mod. Phys. A* **26**, 3918 (2011).
- [45] L. Haiberger, M. Weingran, and S. Schiller, “Highly sensitive silicon crystal torque sensor operating at the thermal noise limit”, *Rev. Sci. Instrum.* **78**, 025101 (2007).
- [46] M. Li, G. W. Mulholland, and M. R. Zachariah, “Rotational diffusion coefficient (or rotational mobility) of a Nanorod in the Free-Molecular Regime”, *Aerosol Sci. Technol.* **48**, 139 (2014).
- [47] C. Zhong, F. Robicheaux, “Shot noise dominant regime of a nanoparticle in a laser beam”, arXiv:1701.04477.
- [48] C. Zhong, and F. Robicheaux, “Decoherence of rotational degrees of freedom”, *Phys. Rev. A* **94**, 052109 (2016).
- [49] B. A. Stickler, B. Papendell, and K. Hornberger, “Spatio-orientational decoherence of nanoparticles”, *Phys. Rev. A* **94**, 033828 (2016)
- [50] M. Li, G. W. Mulholland, and M. R. Zachariah, “The effect of orientation on the mobility and dynamic shape factor of charged axially symmetric particles in an electric field”, *Aerosol Sci. Technol.* **46** (9), 1035 (2012)